Supplementary Information (SI) for Journal of Materials Chemistry B.

In Situ Biocatalytic ATP Regulated, Transient Supramolecular Polymerization

Ananya Mishra, [*a,b] Angshuman Das [a] and Subi J. George[*a]

[a] Supramolecular Chemistry Laboratory, New Chemistry Unit and School of Advanced Materials (SAMat), Jawaharlal Nehru Centre for Advanced Scientific Research (JNCASR), Jakkur, Bangalore 560064, India

[b] Max Plank Bristol Centre for Minimal Biology, Centre for Protolife Research, Centre for Organized Matter Chemistry, School of Chemistry, University of Bristol, Bristol BS81TS, UK. E-mail: ananya.mishra@bristol.ac.uk

Supplementary Figures and Tables

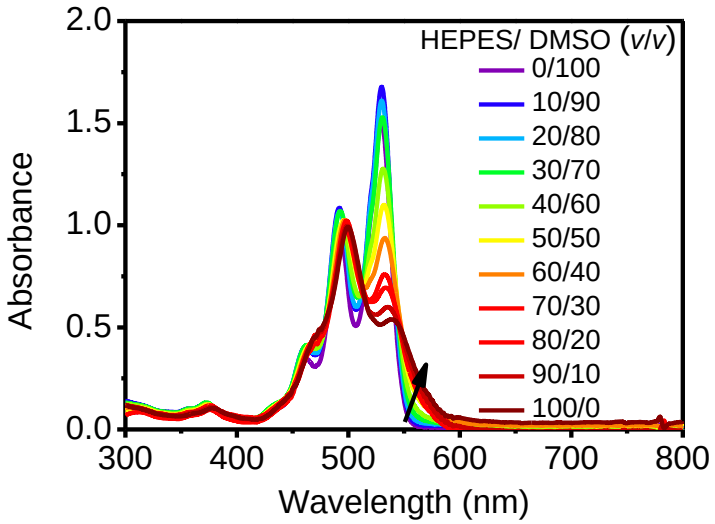

Figure S1: Effect of solvent composition on PDI self-assembly. Composition dependent self-assembly changes ([**PDI**] = 5 x 10^{-5} M, 25 °C).

Note: With increasing the percentage of HEPES in HEPES/DMSO composition of **PDI** solution, a change in ratio of the vibronic bands (A_{492}/A_{530} from 0.64 to 1.48 for 100% DMSO and 100% HEPES, respectively) along with broadening is observed. This indicates towards an increasing aggregating tendency of **PDI** owing to the increase in the percentage of bad solvent (H_2O) in the solution. The observations derived from these results prompted us to perform the following experiments at a composition of HEPES/DMSO (50/50) (*v*/*v*) which is not a highly aggregated state for **PDI** in the absence of any PO_4^{3-} (*vide infra*).

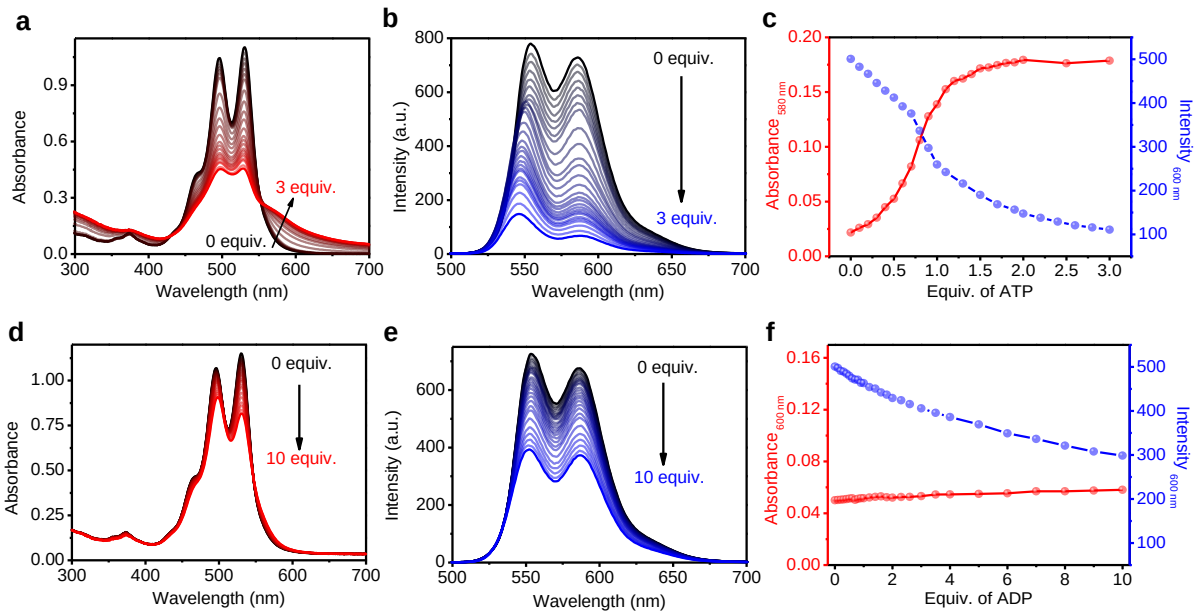

Figure S2: ATP Selective self-assembly of PDI. Absorption (a and d) and emission (b and e) changes of **PDI** with increasing equiv. of ATP (a-c) from 0.0 to 3.0 equiv and ADP (d-f) from 0.0 to 10.0 equiv. c and f) Overlaid titration curves obtained from absorption changes monitored at λ = 580 nm (red) and emission changes monitored at λ = 600 nm (blue) of **PDI** with increasing concentration of ATP (c) and ADP (f) (λ_{ex} = 460 nm, [**PDI**] = 5 x 10^{-5} M, HEPES/DMSO, 50/50, (*v*/*v*), 25 °C).

Note: With addition of increasing concentration of ATP into **PDI** solution mixture, a gradual increase in the aggregate band (monitored at λ = 580 nm) from absorption spectra accompanied with quenching in emission is observed. This is also reflected in the titration curves obtained from both the spectroscopic techniques. Furthermore, a saturation of signal around 2.0 equiv. of ATP is observed indicating saturation of binding sites of **PDI** at this equiv. of ATP. Hence, all the future experiments with ATP were carried out with 2.0 equiv. of ATP. On the contrary, with increasing concentration of ADP we observe negligible changes in the aggregate band of **PDI** as observed from absorption spectra. We also observed less quenching in emission which is reflected in the respective titration curves. These observations indicate that ADP is unable to self-assemble **PDI** effectively even though it binds to the molecule. The reason for such observations is a decreased binding constant of a divalent ADP as compared to a trivalent ATP (Figure S3). Such observations indicate towards a selectivity of **PDI** binding to ATP as compared to ADP.

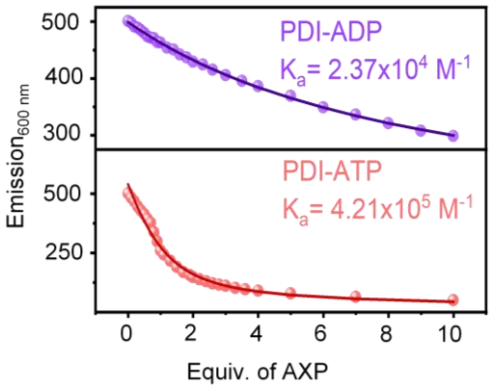

Figure S3: Comparative association constants of PDI-ATP and PDI-ADP. Comparative emission titration curve (λ_{600nm}) of **PDI** bound to ADP (purple curve) and ATP (red curve) fit to 1:1 (H:G) model available on Supramolecular.org through BindFit v0.5 where association constant (K_a) is obtained from the fit curves. The Ka of **PDI-ADP** is calculated as 2.37x10^4 M^{-1} which is less than that of **PDI-ATP** 4.21x10^5 M^{-1} indicating towards stronger binding of ATP with **PDI** leading to efficient aggregation.

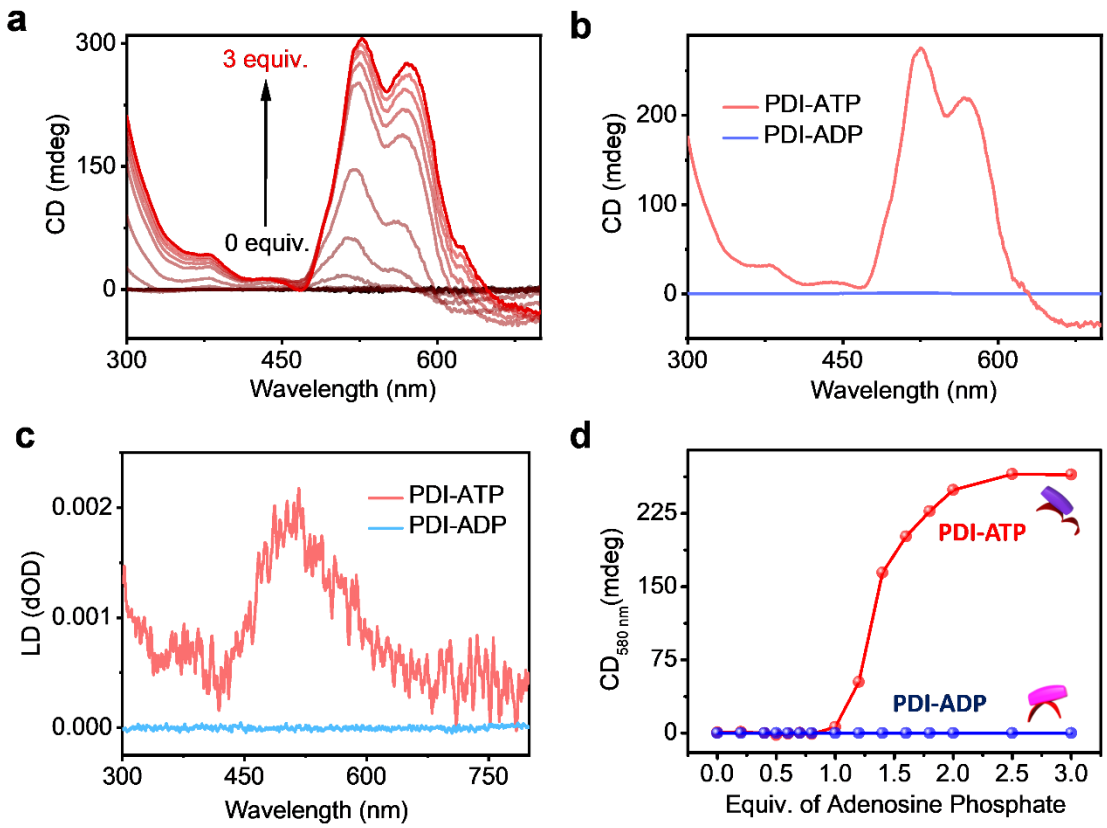

Figure S4: Chirality transmission of adenosine phosphates to PDI self-assembled stacks. a) CD titration curves of **PDI** with increasing equiv. of ATP. b) CD and c) LD spectra of **PDI** with 2 equiv. of ATP (red curve) and ADP (blue curve). d) Comparative titration curves of **PDI** obtained from CD with increasing equiv. of ATP (red curve) and ADP (blue curve) ([**PDI**] = 5 x 10^{-5} M, HEPES/DMSO, 50/50, *v*/*v*, 25 °C).

Note: **PDI** self-assembles selectively on interaction with ATP giving rise to a CD signal while ADP fails to effectively self-assemble **PDI** into helical assemblies. But the absence of a bisignation in the CD signal could be

the result of contamination by the presence of LD. CD signal was observed to be silent until 1.0 equiv. of ATP and a regular increase was seen saturating at 2 equiv. These results indicate that while a small equiv. of ATP (< 1) aggregates **PDI**, it fails to induce chirality to the stacks.

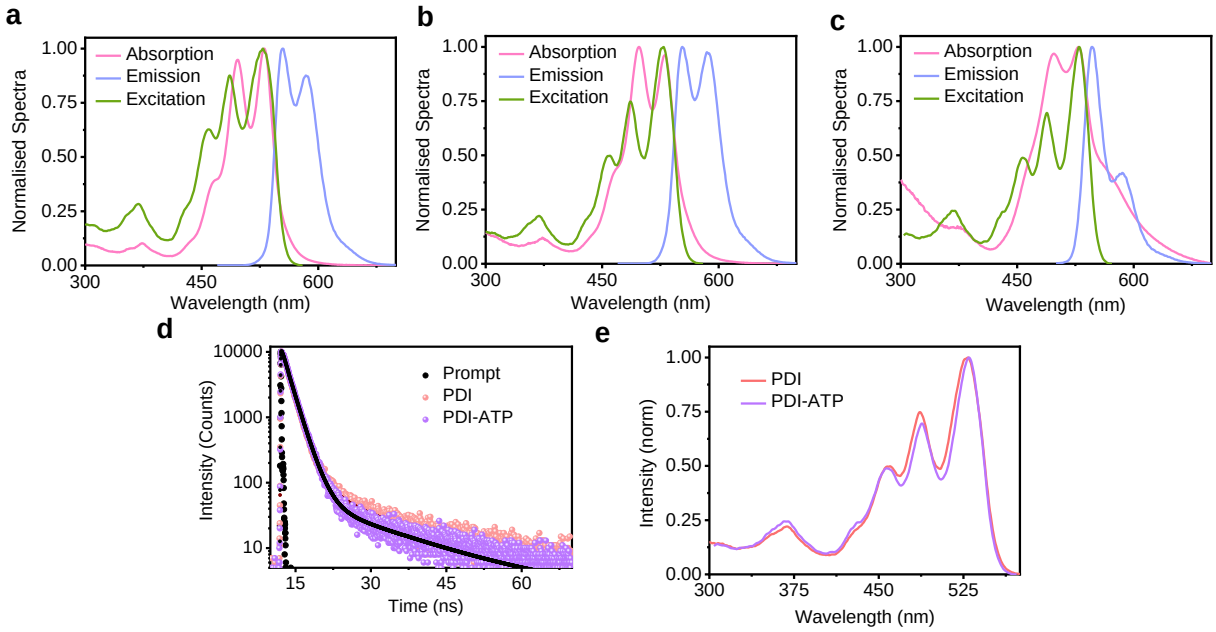

Figure S5: Spectroscopic evidence for ATP induced self-assembly of PDI. Absorption (pink), emission (blue) and excitation (green) spectra of a) **PDI** in HEPES/DMSO (0/100) (*v*/*v*), b) **PDI** in HEPES/DMSO (50/50) (*v*/*v*) and c) **PDI-ATP** in HEPES/DMSO (50/50) (*v*/*v*). Comparative d) lifetime decay profile (λ_{ex} = 442 nm, λ_{coll} = 600 nm) and e) excitation spectra (λ_{coll} = 650 nm) for **PDI** in absence (pink) and presence (purple) of ATP (λ_{ex} = 460 nm, λ_{coll} = 650 nm, [**PDI**] = 5 x 10^{-5} M, HEPES/DMSO, 50/50, (*v*/*v*), 25 °C).

	τ_1	τ_2	τ_3
Without ATP	3.11 ns (89 %)	8.38 ns (5 %)	33.95 ns (6 %)
With ATP	3.01 ns (92 %)	9.89 ns (3 %)	37.66 ns (5 %)

Table S1. Fluorescence life-time values for tri-exponential decay for **PDI** without and with ATP (λ_{ex} = 442 nm, λ_{coll} = 600 nm, [**PDI**] = 5 x 10^{-5} M, HEPES/DMSO, 50/50, (*v*/*v*), 25 °C).

Note: An increase in the aggregate band at 580 nm observed from the normalised absorption spectra is observed in the presence of ATP. The emission observed arises from the residual monomers after ATP induced self-assembly of **PDI**. Furthermore, on collecting the excitation spectra at λ_{coll} = 650 nm, coincides with the absorption spectra indicating towards the formation of H aggregates. All the above results indicate towards the formation of ATP induced H aggregates of **PDI**.

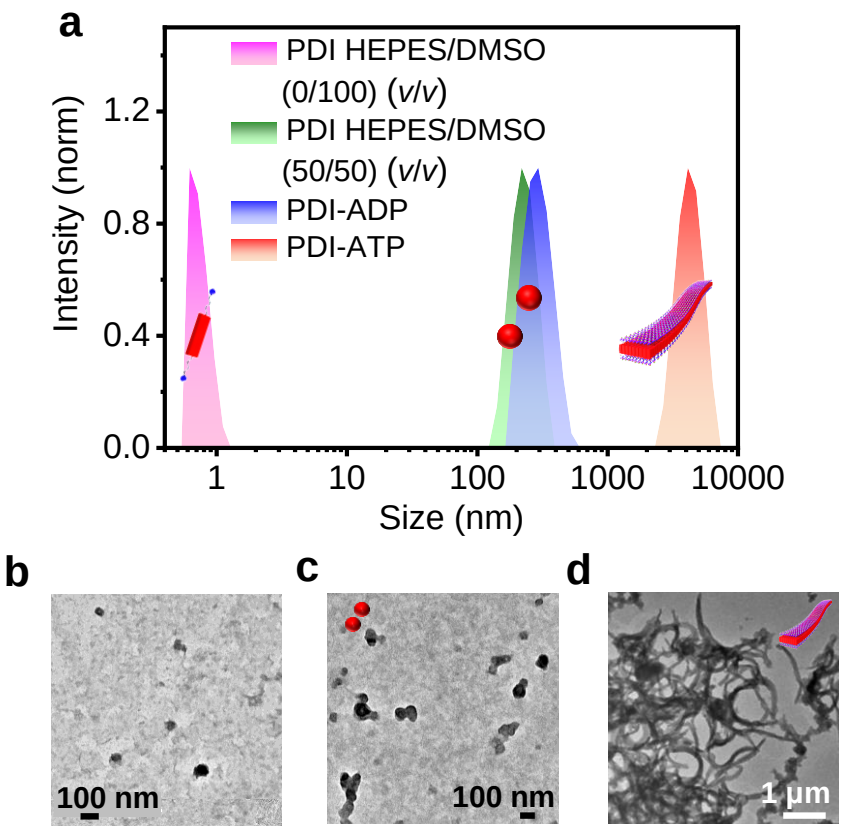

Figure S6: Morphological characterizations of adenosine phosphate induced self-assembled structures of PDI. a) Comparative DLS plot of molecularly dissolved **PDI** (pink), **PDI** in HEPES/DMSO (green), **PDI** bound to 2.0 equiv. of ADP (blue) and 2.0 equiv. of ATP (orange). TEM images of b) **PDI** in HEPES/DMSO, c) 2 equiv. of ADP bound **PDI** and d) 2.0 equiv. of ATP bound **PDI** ([**PDI**] = 5 x 10^{-5} M, H_2O/DMSO, 50/50 (*v*/*v*), TEM stained with uranyl acetate, 1 wt % in water, 25 °C).

Notes: PDI exists in a molecularly dissolved state in DMSO and forms ill-defined small aggregates in HEPES/DMSO 50/50 (*v*/*v*) as well as in presence of ADP. Whereas ATP induces the self-assembly of **PDI** to generate 1D tapes.

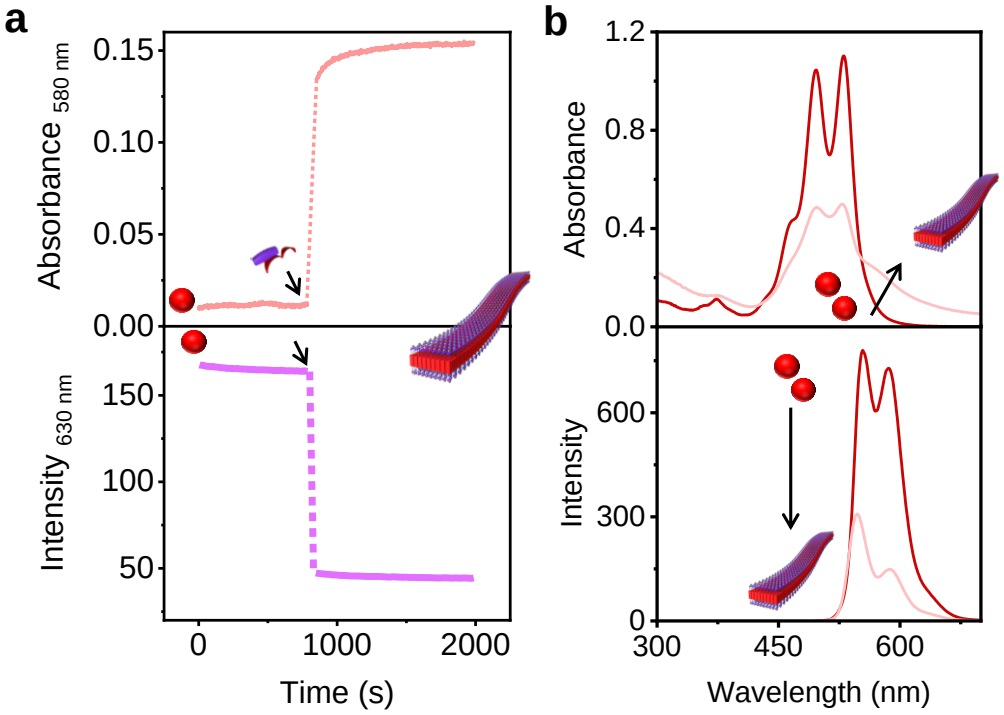

Figure S7: Instantaneous self-assembly of PDI in presence of ATP. a) Time dependent absorbance changes ($\lambda_{580\ nm}$) and emission changes ($\lambda_{630\ nm}$) on addition of 2.0 equiv. of ATP into a solution of **PDI**. b) Comparative absorption and emission spectra before and after addition of ATP into a solution of **PDI** ([**PDI**] = 5 x 10^{-5} M, HEPES/DMSO, 50/50, (*v*/*v*), 25 °C).

Notes: No temporal control over the self-assembly process is observed when ATP is introduced to a solution of **PDI**. These spectroscopic results indicate that the ATP induced aggregation process of **PDI** is instantaneous.

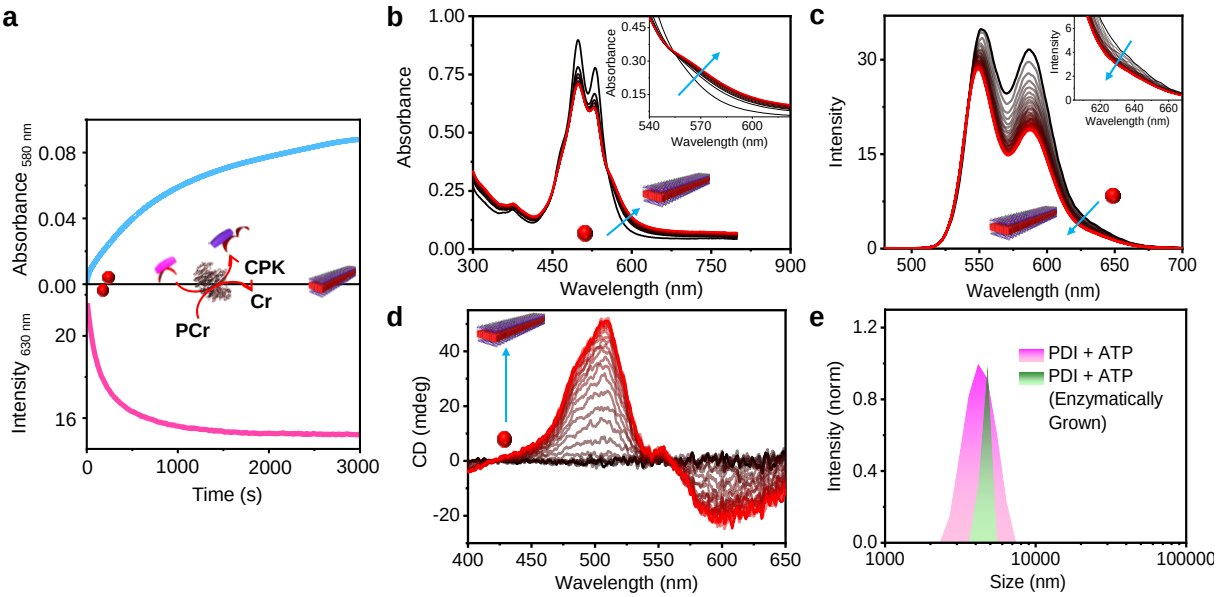

Figure S8: Temporal control over PDI self-assembly. a) Time dependent absorbance changes (blue, $\lambda_{580\ nm}$) and emission changes (pink, $\lambda_{630\ nm}$) resulting from ATP driven self-assembly of **PDI** as ADP enzymatically converts to ATP in presence of enzyme CPK and using PCr as substrate. Spectroscopic evolution of b) absorbance, c) emission and d) CD as **PDI** self-assembles over 3000s as ATP is enzymatically produced *in situ*. e) Comparative DLS profile of instantaneously and enzymatically grown ATP bound **PDI** ([**PDI**] = 5 x 10^{-5} M, ADP = 2.0 equiv., CPK =15.0 U/mL, PCr = 10.0 equiv., HEPES/DMSO, 50/50, (*v*/*v*), 25 °C).

Note: Time dependent spectroscopic trace obtained for enzymatically grown ATP bound **PDI** shows a gradual increase in the aggregate band at $\lambda_{580\ nm}$ in absorption along with an overall quenching in emission. CD spectra show a temporal evolution of bisignated signal (λ=540 nm) indicating towards a reduced effect of LD. The DLS spectra shows a narrower dispersity for the enzymatically grown tapes as compared to the instantaneously grown tapes. All these results indicate towards the controlled self-assembly process of **PDI** when ATP is slowly released which fuels its aggregation into tapes of controlled dimensions.

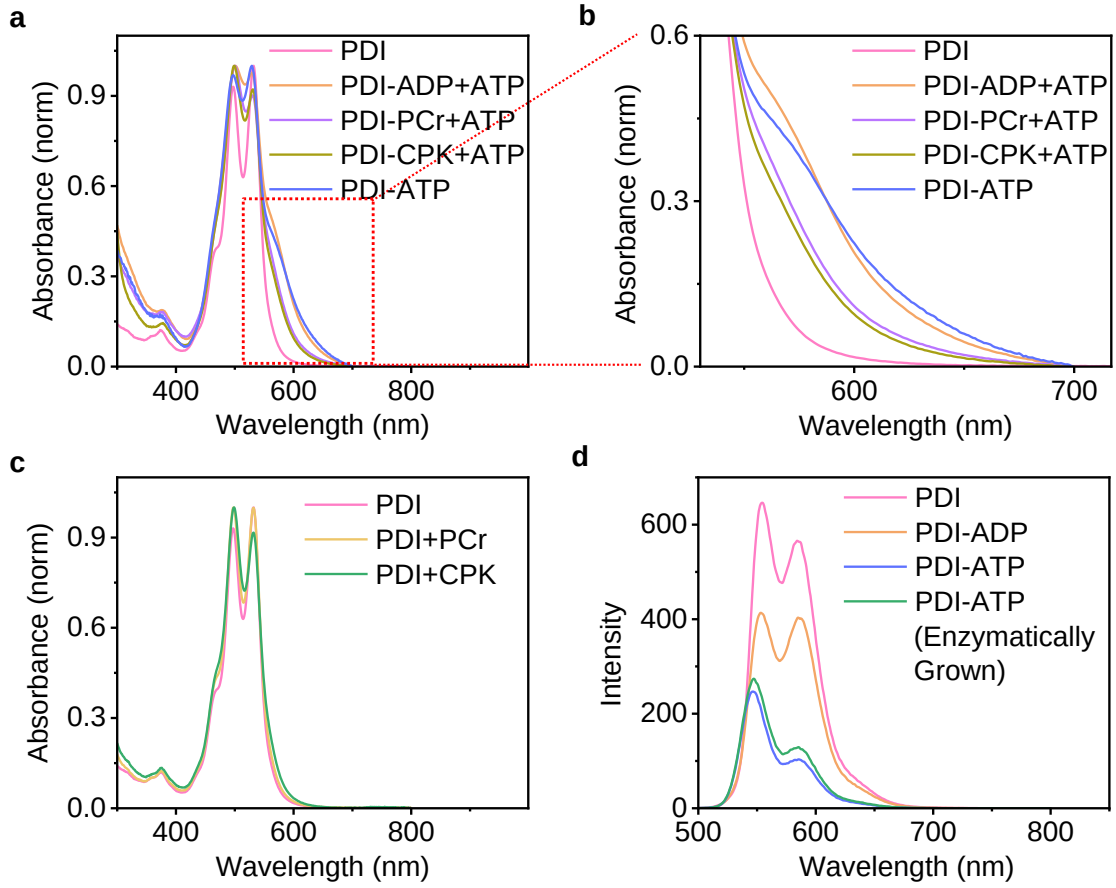

Figure S9: Spectroscopic evidence of PDI self-assembly. Comparative normalised absorption (a) and zoomed in absorption (b) spectra showing **PDI** and **PDI**-ADP, **PDI**-PCr, **PDI**-CPK to which 2.0 equiv. of ATP was added and **PDI**-ATP. c) Normalised absorbance of **PDI**, **PDI**+PCr and **PDI**+CPK. d) Comparative emission of **PDI**, **PDI**-ADP, **PDI**-ATP and **PDI** bound to enzymatically grown ATP. ([**PDI**] = 5 x 10^{-5} M, CPK =15.0 U/mL, PCr = 10.0 equiv., ADP= 2.0 equiv., ATP= 2.0 equiv., HEPES/DMSO, 50/50, (*v*/*v*), 25 °C).

Note: When 2.0 equiv. of ATP was added to a solution of ADP bound **PDI** it shows a jump in the aggregate band which corresponds to the **PDI**-ATP indicating that the added ATP completely replaces bound ADP owing to trivalent interaction of **PDI** with ATP. PCr and CPK themselves are unable to induce any effective aggregation as seen from the absence of an aggregate band in case of PCr or CPK bound **PDI**. On addition of 2.0 equiv. of ATP to PCr or CPK bound **PDI** an increase in aggregate band is observed but it is not to the same extent as nascent **PDI**-ATP. So, fresh feed of ATP replaces any PCr and CPK bound to **PDI** but the aggregation mode and the resulting spectroscopic properties are affected by the environment. Furthermore, emission shows that the resultant emission for enzymatically grown tapes of **PDI**-ATP is similar to nascent **PDI**-ATP. All these experiments indicate that though the extent of growth in enzymatically grown stacks of **PDI**-ATP does not correspond to the nascent **PDI**-ATP, but assembly occurs over time to result in one dimensional structure similar to tapes as seen in nascent **PDI**-ATP.

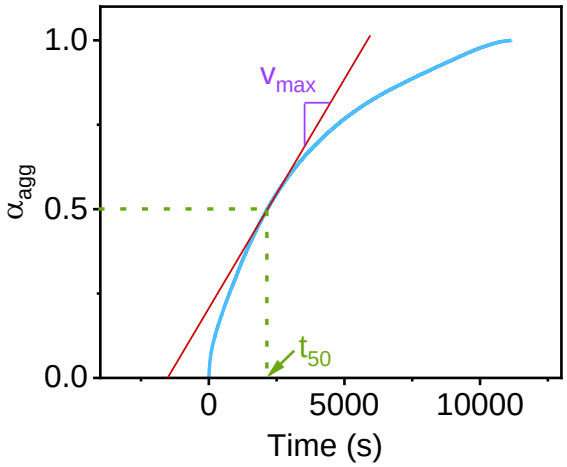

Figure S10: Calculation of time parameters for enzymatically triggered temporal self-assembly of PDI. The temporal self-assembly process of **PDI**-ATP was analysed to obtain various time parameters from the elongation process. We calculated t_{50}(half-time i.e. time required for completion of 50% of the process) from tangent drawn at the inflection point (time at which growth rate reaches its maximum i.e. v_{max}). t_{50} and v_{max} was calculated plotted for various concentrations of ADP, PCr and CPK to obtain a trend.

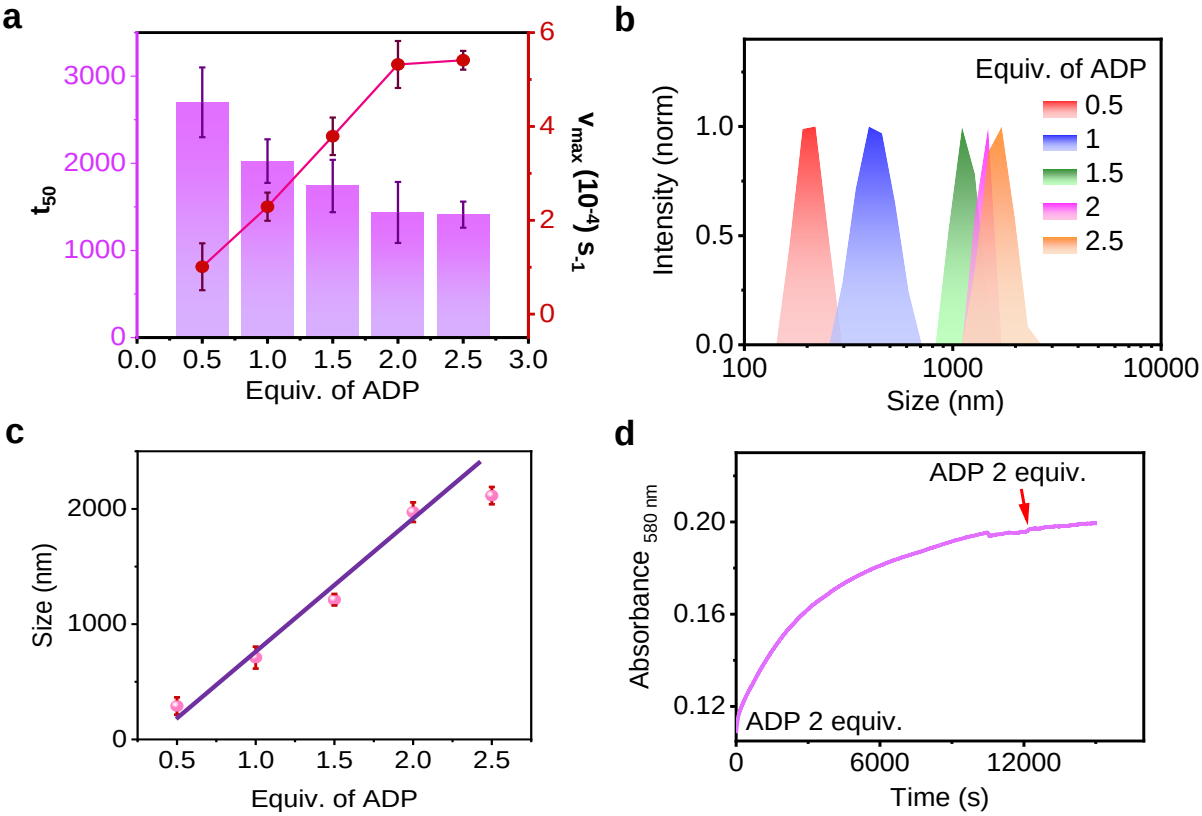

Figure S11: Enzymatically ATP generation from different concentration of ADP. a) Comparative plots showing the trends of t_{50} and v_{max} obtained from time profile of enzymatic generation of ATP for varying concentrations of ADP leading to **PDI** self-assembly. b) DLS and c) size profile showing the increase in size when ATP bound **PDI** is enzymatically grown from varying equiv. of ADP. d) Time dependent absorbance changes monitored at λ_{580nm} for enzymatically grown **PDI**-ATP starting with 2.0 equiv. of ADP where another batch of 2.0 equiv. of ADP was added after complete elongation. ([**PDI**] = 5 x 10^{-5} M, CPK = 15 U/mL, PCr = 10 equiv., HEPES/DMSO, 50/50, *v*/*v*, 25 °C).

Note: With an increasing concentration of ADP, a faster production of ATP leads to faster kinetic profiles of **PDI** self-assembly leading to a decrease in t_{50} values and an increase in v_{max}. Straight line fit shows size increase of enzymatically grown tapes with increasing concentration of ADP. Enzymatic conversion of ADP to ATP in presence of CPK (enzyme) and PCr (substrate) produces equivalent amount of ATP from introduced equiv. of ADP. So, on addition of a second batch of 2.0 equiv. of ADP to an already grown stack grown with 2.0 equiv. of ADP, shows no further elongation as 2.0 equiv. of ATP saturates the binding sites of **PDI**.

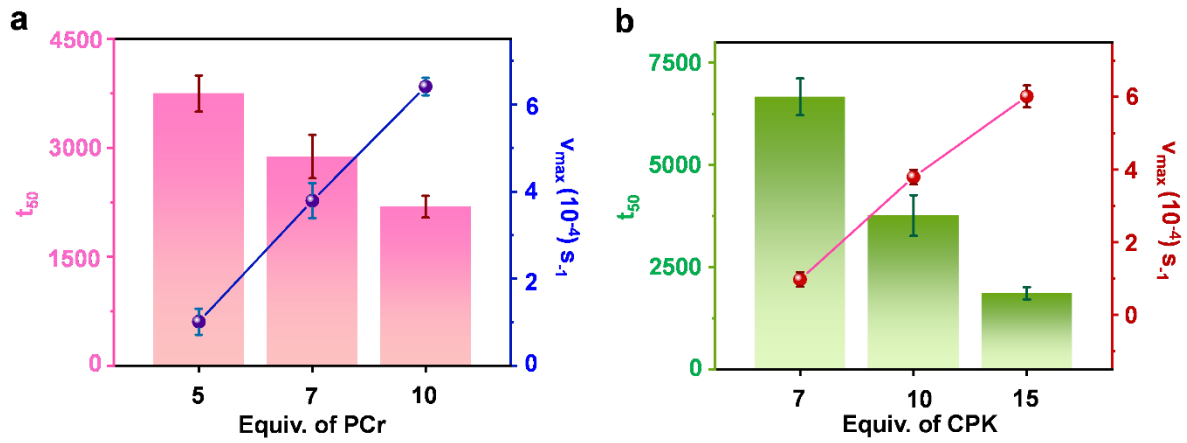

Figure S12: Enzymatic ATP generation from different concentration of PCr and CPK. Comparative plots showing the trends of t_{50} and v_{max} obtained from time profile of enzymatic generation of ATP for varying concentrations of a) PCr at 2 equiv. ADP and 15 U/mL CPK and varying concentrations of b) CPK at 10 equiv. of PCr, 2 equiv. of ADP for **PDI** aggregation. ([**PDI**] = 5 x 10^{-5} M, HEPES/DMSO, 50/50, *v*/*v*, 25 °C).

Note: With increasing concentration of PCr in the solution (substrate for the enzymatic conversion of ADP to ATP), there is an increase in the amount of PO_4^{3-} generated in the solution which can enzymatically react with ADP to generate ATP. This in turn affects the extent of growth of enzymatically controlled ATP bound **PDI**. Moreover, increasing concentration of CPK triggers a faster enzymatic generation of ATP and in turn a faster **PDI** self-assembly. This leads to a decreasing t_{50} and an increasing v_{max}.

All the above results obtained by varying the concentration of the substrates ADP and PCr and the units of CPK have been shown to affect the self-assembly kinetics of **PDI**. Since the aggregation of **PDI** to one dimensional tape occurs only in the presence of ATP, we can safely deduce that there is an *in situ* enzymatically controlled generation of ATP which in turn directly controls the self-assembly process. By simple modifications of the environment, we could successfully tweak the self-assembly extent as well as the self-assembly kinetics.

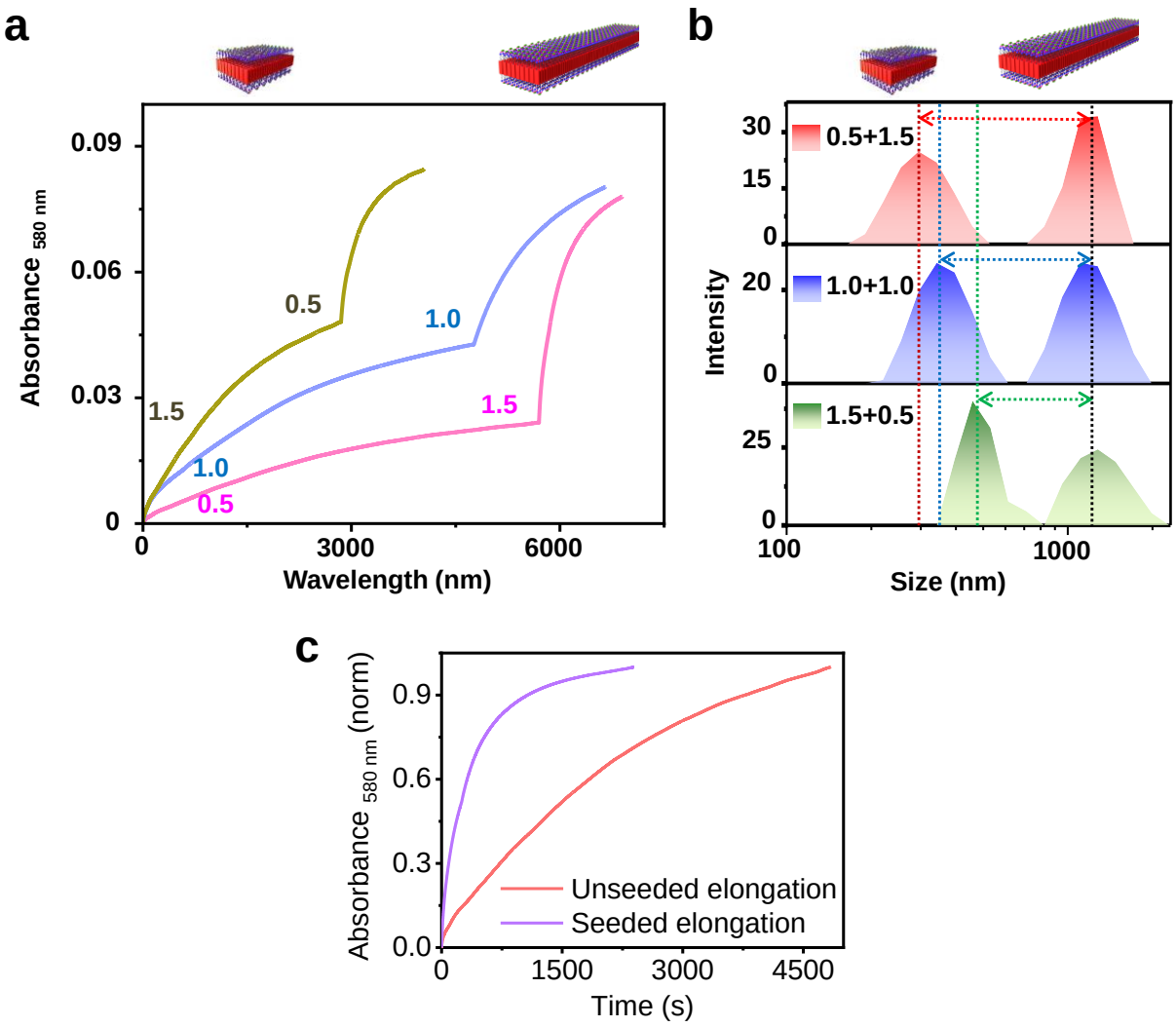

Figure S13: Seeding experiments through enzymatically generated ATP. a) Absorbance changes monitored at $\lambda_{580\ nm}$ and b) DLS changes monitored for sequential addition of ADP for enzymatic elongation of **PDI**. (Numbers indicate the equiv. of ADP added in each batch) ([**PDI**] = 5 x 10^{-5} M, CPK = 15.0 U/mL, PCr = 10.0 equiv., HEPES/DMSO, 50/50, v/v, 25 °C). c) Normalised overlaid elongation kinetics obtained from absorbance changes for unseeded (red plot) and seeded growth (blue plot). ([**PDI**] = 5 x 10^{-5} M, each ADP batch = 0.2 equiv., CPK = 15.0 U/mL, PCr = 10.0 equiv., HEPES/DMSO, 50/50, *v*/*v*, 25 °C).

Note: Seeded elongation appears to be kinetically faster than the unseeded elongation leading to an increase in size. This observation further confirms growth of the one-dimensional tape from the ends of seed due to the second batch addition of ADP.

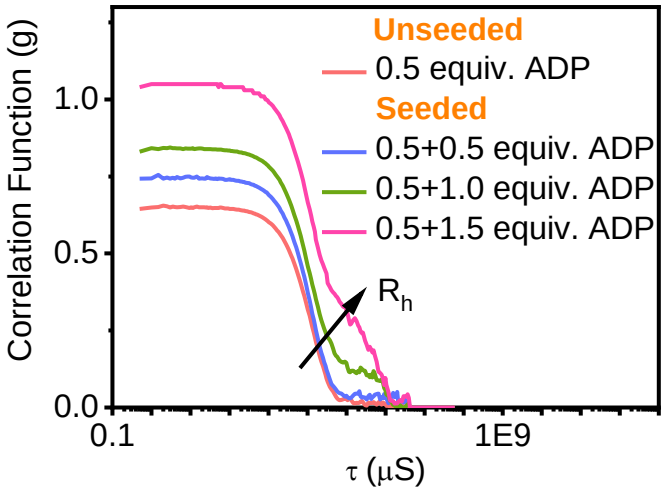

Figure S14: Size changes obtained from seeding experiments in enzymatic elongation of PDI. Correlation function change derived directly from DLS obtained for seed and seeded enzymatic elongation of **PDI** by batch-wise addition of ADP ([**PDI**] = 5 x 10^{-5} M, first batch ADP = 0.5 equiv., second batch ADP = 0.5, 1.0 and 1.5 equiv., CPK = 15.0 U/mL, PCr = 10.0 equiv., HEPES/DMSO, 50/50, *v*/*v*, 25 °C).

Note: An increase in size is observed from unseeded tapes to seeded tapes with increasing concentration of ADP added in the second batch. The mean value of the size increase follows a linear change. Since the size increase data has been obtained from DLS experiments, we obtained the correlation function change for unseeded (red curve) and seeded data, which shows an increase in lag time on seeding which further indicates towards an increase in size with increase in scattering on seeding. These observations indicate controlled supramolecular polymerization reaction with good quality correlation curves from DLS.

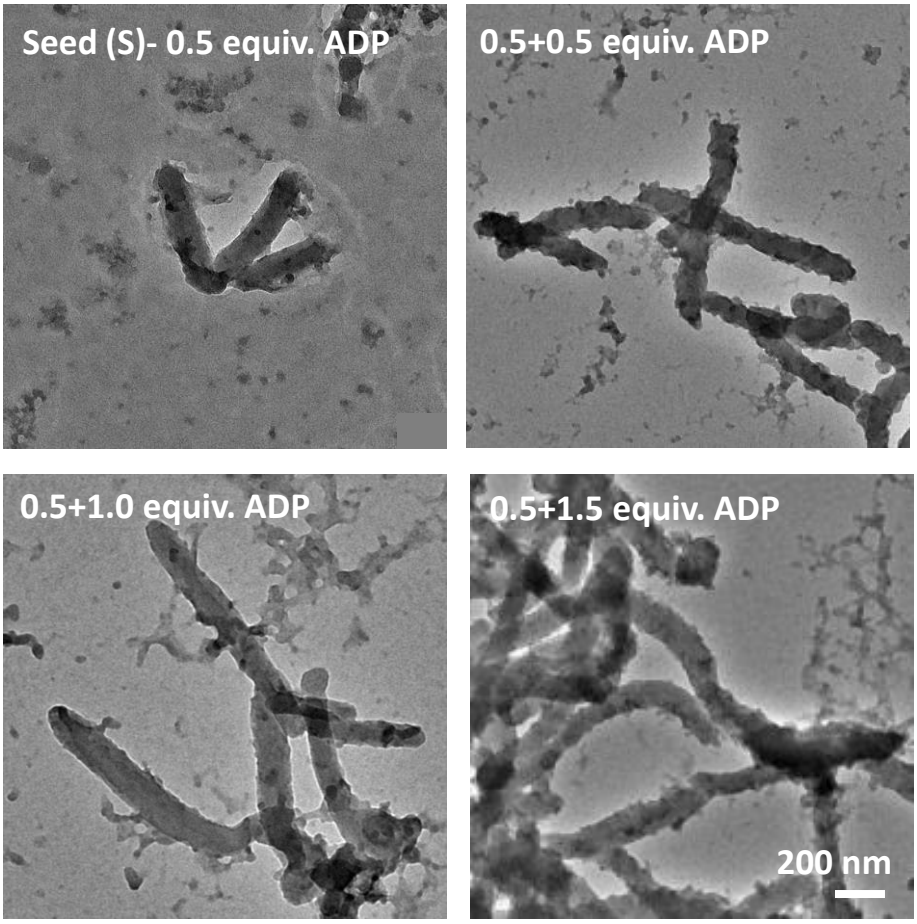

Figure S15: Morphological characterization of seed and seeded PDI tapes. TEM images obtained for a) seed (first batch ADP = 0.5 equiv.) and seeded (second batch ADP = b) 0.5, c) 1.0 and d) 1.5 equiv.) enzymatic elongation of **PDI** by batch-wise addition of ADP. ([**PDI**] = 5 x 10^{-5} M, CPK = 15.0 U/mL, PCr = 10.0 equiv., H_2O/DMSO, 50/50, *v*/*v*, 25 °C).

Note: An increase in size is observed from unseeded (first batch ADP added = 0.5 equiv.) to seeded tapes (second batch ADP added = 0.5, 1.0 and 1.5 equiv.) from the TEM images. Due to the overlap in most tapes individual dimensions could not be obtained for constructing a histogram even though a clear increase in dimensions is observed. Instead DLS data has been utilized to give an idea regarding the size increase on seeding.

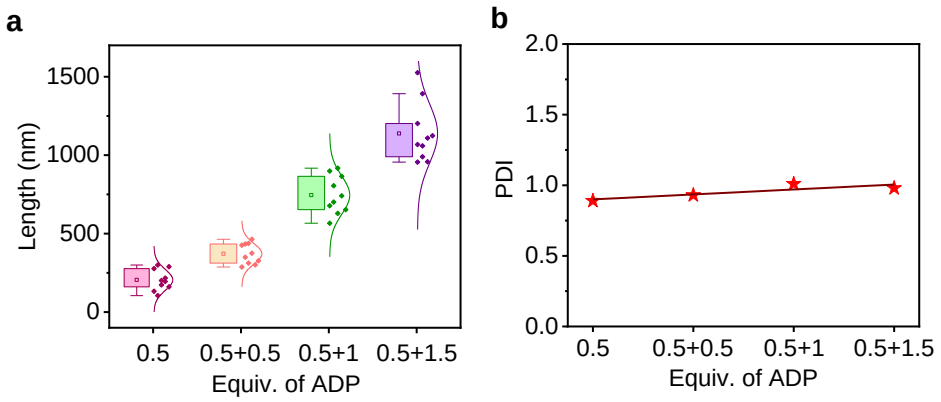

Figure S16: Size distribution and polydispersity of seeded self-assembly of PDI-ATP. a) Size distribution with box plot and the individual sizes analysed for 10 distinct enzymatically grown tapes from TEM images for 0.5 equiv. of ADP (pink) and for seeded assembly with 0.5+0.5 (orange), 0.5+1.0 (green) and 0.5+1.5 (purple) equiv. of ADP. b) Polydispersity Index (PDI) calculated from the 10 tapes analysed from TEM images. PDI was calculated using the formula $PDI = \frac{Lw}{Ln}$ where L_w is weight average length and L_n is number average length.

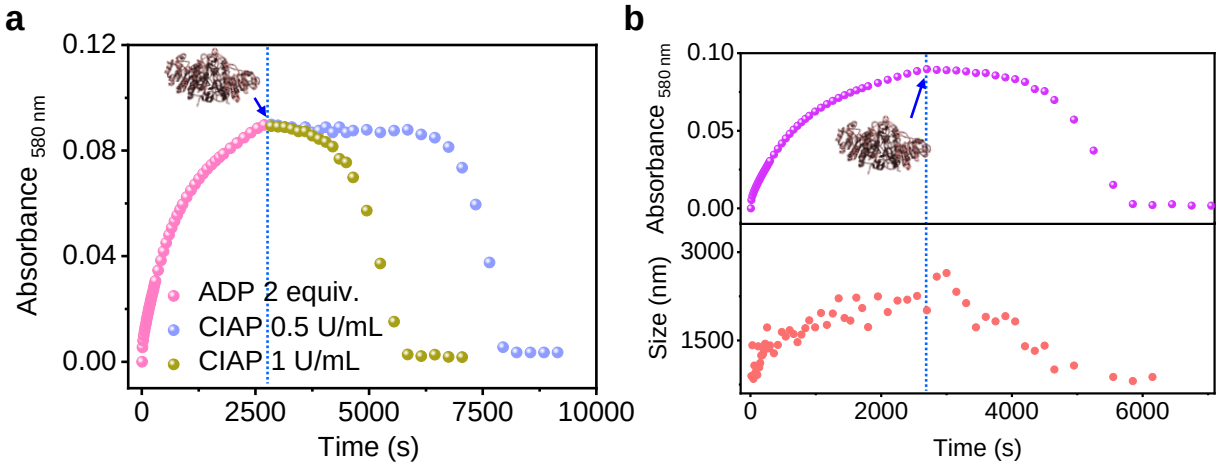

Figure S17: Passive cycle for PDI self-assembly followed by disassembly by enzymatic ATP regulation. a) Absorbance changes monitored at $\lambda_{580\ nm}$ showing the elongation kinetics and disassembly for two concentrations of CIAP and b) co-stacked absorbance and scattering changes (CIAP = 1.0 U/mL) showing passive assembly of **PDI**-ATP indicating growth followed by disassembly after CIAP is added into solution containing elongated stacks ([**PDI**] = 5 x 10^{-5} M, ADP = 2.0 equiv., CPK = 15.0 U/mL, PCr = 10.0 equiv., HEPES/DMSO, 50/50, v/v, 25 °C).

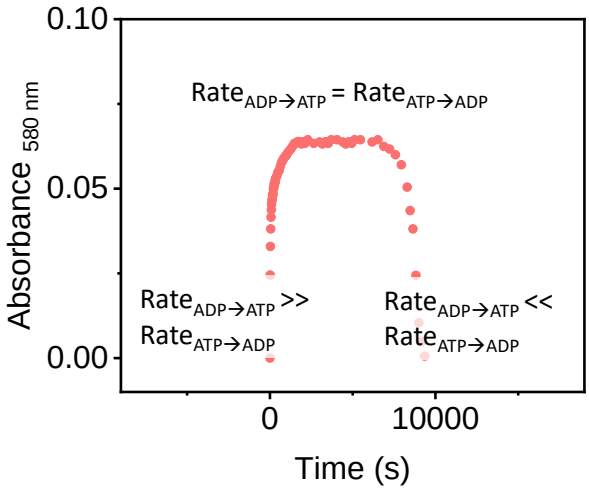

Figure S18: ATP regulation reaction leading to various kinetic states of PDI-ATP assembly. Representative graph showing the overall transient process for **PDI** aggregation. The initial increase in absorbance indicates the self-assembly process of **PDI** as ATP is generated *in situ* enzymatically. Though ATP hydrolysis also occurs, the rate of ATP generation is faster than ATP hydrolysis. A steady state is reached which indicates towards an equal ATP generation and consumption rate. Following this, the rate of ATP hydrolysis overtakes ATP generation as ADP is consumed and a decrease in absorbance is observed. This overall process is controlled by varying the concentrations of substates and enzymes involved in the process.

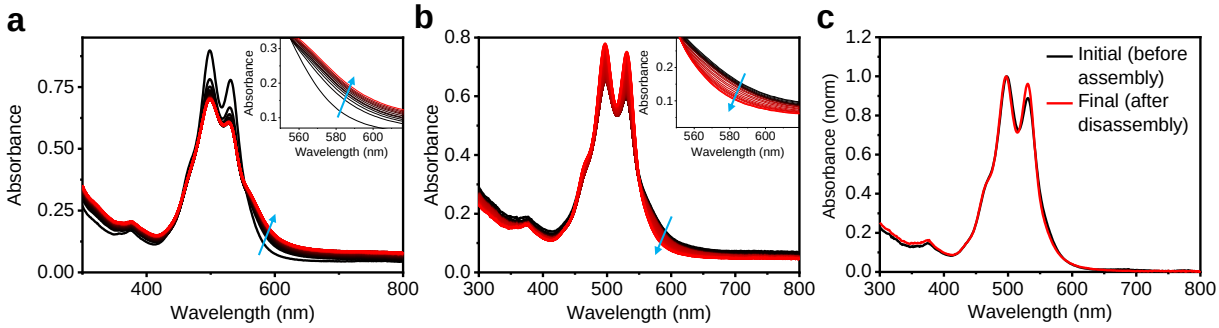

Figure S19: Spectroscopic evidence for PDI self-assembly and disassembly by enzymatic ATP regulation. Absorbance spectral changes during a) assembly and b) disassembly and c) comparison of absorbance spectra for t_0 during assembly and t_{final} after disassembly of a transient assembly of **PDI**-ATP, where the insets shows the corresponding change at aggregated band. ([**PDI**] = 5 x 10^{-5} M, ADP = 2.0 equiv., CPK = 20.0 U/mL, PCr = 4.0 equiv., HEPES/DMSO, 50/50, *v*/*v*, 25 °C).

Note: The absorbance spectra obtained at t_0 state of assembly and t_{final} state of disassembly obtained for a transient self-assembly process is shown to coincide. This indicates that the states reached after the completion of a transient state is same as that of the beginning of the cycle.

CIAP Units (U/mL)	Assembly Rate (dA/dT) (min^{-1})	Assembly Lifetime (min)	Dis-assembly Rate (dA/dT) (min^{-1})	Dis-assembly Lifetime (min)	Transient state lifetime (min)	Amplitude (Absorbance at 580 nm)
0.2	3.19×10^{-4}	160	7.97×10^{-5}	640	480	0.051
0.3	3.21×10^{-4}	140	9.57×10^{-5}	470	330	0.045
0.4	3.27×10^{-4}	96	12.5×10^{-5}	294	330	0.037

Table S2: Parameters derived regarding rate of assembly, disassembly and lifetimes derived from the transient cycle for varying units of CIAP ([**PDI**] = 5×10^{-5} M, ADP = 2.0 equiv., CPK = 20.0 U/mL, PCr = 4.0 equiv., HEPES/DMSO, 50/50, *v*/*v*, 25 °C).

Note: From the above parameters got from the transient assembly experiments we notice that by keeping the concentration of CPK constant, the rate of assembly is hardly affected with varying CIAP concentrations. CIAP only affects the extent of assembly, i.e. higher the concentration of CIAP, lesser the extent of assembly. This is seen because higher units of CIAP start hydrolysing the produced ATP faster hence preventing further growth. This further affects the assembly lifetime i.e. a decrease in lifetime is seen with increasing CIAP. Since CIAP is an ATP hydrolysing enzyme, small changes in its concentration affects the rate of disassembly as well as its lifetime considerably. Higher the concentration of CIAP, faster is the observed disassembly process. Along with these observations, transient state lifetime as well as amplitude of growth is affected by concentration of CIAP. Hence, higher CIAP units result in smaller amplitude of growth and transient state lifetime.

Cycles	Assembly Rate (dA/dT) (min^{-1})	Assembly Lifetime (min)	Dis-assembly Rate (dA/dT) (min^{-1})	Dis-assembly Lifetime (min)	Transient state lifetime (min)	Amplitude (Absorbance at 580 nm)
1	6.94×10^{-4}	108	4.17×10^{-4}	180	242	0.075
2	8.7×10^{-4}	46	1.29×10^{-4}	310	194	0.04

Table S3: Parameters derived regarding rate of assembly, disassembly and lifetimes derived from the transient cycle for varying units of CPK ([**PDI**] = 5×10^{-5} M, First addition (ADP = 2.0 equiv., PCr = 4.0 equiv.), Second addition (ADP = 4.0 equiv., PCr = 8.0 equiv.), CPK = 20.0 U/mL, CIAP = 0.4 U/mL, HEPES/DMSO, 50/50, *v*/*v*, 25 °C).

Note: The second cycle sees retarded amplitudes, rates as well as lifetime which could be the result of build-up of waste PO_4^{3-} in the solution due to the hydrolysis process.